

# Nucleation at liquid | liquid interfaces: electrodeposition without electrodes

Christoffer Johans<sup>a</sup>, Riikka Lahtinen<sup>a</sup>, Kyösti Kontturi<sup>a,\*</sup>, David J. Schiffrin<sup>b</sup>

<sup>a</sup> Department of Chemical Technology, Laboratory of Physical Chemistry and Electrochemistry, Helsinki University of Technology, PO Box 6100, Kemistintie 1, FIN-02150-HUT Espoo, Finland

<sup>b</sup> Department of Chemistry, Donnan and Robert Robinson Laboratories, University of Liverpool, Liverpool L69 3BX, UK

Received 13 February 2000; received in revised form 24 May 2000; accepted 29 May 2000

## Abstract

A model has been developed for diffusion controlled electrodeposition of metallic particles at the interface between two immiscible electrolyte solutions. A rate law was derived for the case where no preferential nucleation sites are present. Palladium particles were deposited at the water | 1,2-dichloroethane interface by reduction of aqueous ammonium palladate using butylferrocene in the organic phase as electron donor. Experimental results were in good agreement with the theoretical model derived. The potential dependence of the nucleation rate was found to follow a classical exponential law. © 2000 Elsevier Science S.A. All rights reserved.

**Keywords:** ITIES; Electrodeposition; Palladium; Nucleation; Nanoparticles

## 1. Introduction

The advantage of studying nucleation phenomena by electrochemical techniques is that the supersaturation can be controlled by the applied interfacial potential. In 1996 Cheng and Schiffrin [1] nucleated gold particles at a polarisable liquid | liquid interface. The basic concepts of nucleation and growth at a liquid | liquid interface are essentially similar to those at a solid electrode, i.e. formation of a nucleus, which grows after reaching a critical size [2]. The nucleation process at a solid electrode is affected by the interaction between the newly formed phase and the electrode substrate. The main difference when nucleation takes place at a liquid | liquid interface is that, for the latter, this interaction is very small. In addition, the liquid | liquid interface should be free from defects serving as permanent preferential nucleation sites, thus making it an ideal substrate for interfacial nucleation studies.

The growth of each nucleus is determined by the rate of incorporation of new atoms, and for fast kinetics

mass transfer controls growth. As growth proceeds the diffusional fields overlap and the diffusional geometry changes from hemispherical to linear. This is a very complex problem and an exact solution cannot be obtained. Scharifker and co-workers [3–5] introduced the idea of planar diffusion zones to approximate the expected current. The applicability of this approach is still under debate [6]. Mirkin and Nilov [7], Sluyters-Rehbach et al. [8] and Heerman and Tarallo [6] have suggested some refinements to the model and more recently Scharifker et al. [9] have scrutinised the theoretical aspects of these approaches in comparison with numerical simulations.

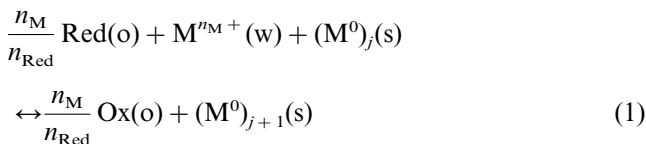
Modelling nucleation and growth phenomena at liquid | liquid interfaces requires that diffusion in both phases must be considered, since the charge transfer in these systems occurs by transport of electroactive species to the interfacial region from both phases. The diffusional fields thus generated are coupled and the diffusional problem in both adjoining phases must be solved. This paper presents a nucleation and growth model for the liquid | liquid interface based on the concept of planar diffusion zones. The experimental results are compared to model predictions.

\* Corresponding author. Tel.: +358-9-4512575; fax: +358-9-4512580.

E-mail address: kontturi@pop.hut.fi (K. Kontturi).

## 2. Theory

The immiscible electrolyte system that is being considered consists of an organic solvent immiscible with water containing an organic redox couple, in contact with an aqueous solution of a metal ion. By applying a suitable interfacial Galvani potential difference, heterogeneous electron transfer from the organic redox couple to the aqueous metal ion takes place, leading to the electrodeposition of a metal phase at the interface. This type of electrodeposition experiment has been carried out with gold [1] and is equivalent to classical electrodeposition at a solid electrode. The nucleation and growth reaction can be written as:



where Red and Ox denote the reduced and oxidised components of the electron donor redox couple.  $n_{\text{Red}}$  is the number of electrons transferred from the organic redox couple and  $n_M$  is the number of electrons required to reduce the metal ion.  $j$  is the number of atoms in the growing particle.  $n_{\text{Ox}}$  is used in several equations and is defined as  $n_{\text{Ox}} = -n_{\text{Red}}$  for convenience, where the negative sign denotes that Ox is a reaction product.

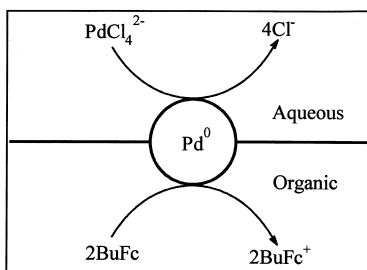


Fig. 1. Schematic presentation of the electrochemical reduction of palladate at the liquid|liquid interface. Two electrons are transferred from the organic butylferrocene redox couple to reduce the palladate.

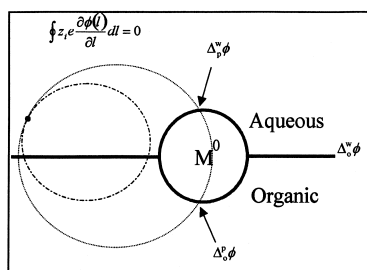


Fig. 2. Schematic diagram showing the transfer of an idealised test charge across any closed loop at the liquid|liquid interface in the presence of a metallic particle. Since the work for any closed loop has to be zero, the overall driving force for the deposition reaction must equal the potential across the interface.

For a reversible reaction the two-phase Nernst equation that defines the interfacial potential is given by [10]:

$$\Delta_{\text{o}}^{\text{w}}\phi = E_{\text{Red/Ox}}^{\text{o}} - E_{\text{M}^0/\text{M}^{n_M}}^{\text{o}} + \frac{RT}{n_{\text{Red}}n_M F} \ln\left(\frac{c_{\text{Ox(o)}}^{\sigma} c_{\text{M}^0}^{\sigma}}{c_{\text{Red(o)}}^{\sigma} c_{\text{M}^0}^{\sigma} c_{\text{M}^0(\text{w})}^{\sigma n_M}}\right) \quad (2)$$

where  $E_{\text{Red/Ox}}^{\text{o}}$  and  $E_{\text{M}^0/\text{M}^{n_M}}^{\text{o}}$  are the formal potentials of the organic and aqueous redox couples referred to the standard hydrogen electrode in the respective phases. These values include all activity coefficient terms. The superscript  $\sigma$  denotes surface concentration. The activity of the metal in the particle is assumed to be unity and the formal redox potential of the metal couple is assumed to be independent of size, although density functional calculations of aluminium clusters imply a pronounced change in the binding energy per atom for clusters comprised between one and thirteen atoms [11]. The size of the cluster considered here, is much larger than this and electronic size effects have been neglected. The overpotential  $\eta$  is defined as:

$$\eta = \Delta_{\text{o}}^{\text{w}}\phi - \Delta_{\text{o}}^{\text{w}}\phi_{\text{eq}} \quad (3)$$

where  $\Delta_{\text{o}}^{\text{w}}\phi_{\text{eq}}$  is the equilibrium potential for the reaction.

Care has to be taken in analysing electrodeposition at liquid|liquid interfaces in relation to the physical meaning of the overpotential experienced by a cluster present at the interface. The situation here differs from that at a solid electrode since there is no electronically conducting substrate and the electron donor is a soluble redox species. Therefore, the process has some similarities with homogeneous nucleation of particles. Fig. 1 illustrates the reaction that takes place. A central issue that needs understanding is the actual driving force experienced by a growing particle at the interface. For a metal|solution interface, the problem can be easily defined since the potential experienced by the new growing phase is that of the electrode and therefore, the growth overpotential is clearly defined. For a liquid|liquid interface, the electrode surface is a dielectric termination and not a conductor.

The nature of the potential distribution can be considered from the analysis given in Fig. 2. A fundamental relationship that must be valid for the transfer of a test charge along any pathway across the interface, irrespective of whether the particle is crossed or not, is that the line integral:

$$\oint_{z,e} e \frac{\partial \phi(l)}{\partial l} dl = 0 \quad (4)$$

i.e. the energy resulting from transferring an idealised test charge across any closed loop, must be zero.  $z,e$  is the test charge,  $\phi(l)$  is the potential at any point in the loop and  $l$  is the integration variable. The use of Eq. (4) implies that the Galvani (or 'inner') potential is a measurable quantity. We are employing this concept

here due to the need to use an electrical variable in order to define an electrochemical nucleation and growth supersaturation. A consequence of this is that a growing particle, which by its metallic nature must be an equipotential, behaves as a bipolar electrode in which the sum of the interfacial potential drops at the water | particle and the particle | organic solution interfaces must equal the total interfacial Galvani potential difference across the liquid | liquid interface, i.e.:

$$\Delta_{\text{p}}^{\text{w}}\phi + \Delta_{\text{o}}^{\text{p}}\phi = \Delta_{\text{o}}^{\text{w}}\phi \quad (5)$$

where the index p refers to the particle. It follows that the overall driving force for the deposition reaction is the potential across the interface.

The mass transfer equations for a single growing particle can be solved using the following assumptions:

1. the particle is spherical;
2. hemispherical diffusion applies in both phases;
3. no convective term due to particle growth is considered;
4. the mass balance condition is that the total flux of reducing agent from the organic phase equals that of metal ions being deposited on the growing nuclei;
5. the diffusional field may be regarded to be in a quasi-stationary state provided that it develops much faster than the rate of particle growth.

With these assumptions the diffusional equations are:

$$D_i \left( \frac{\partial^2 c_i}{\partial r^2} + \frac{2}{r} \frac{\partial c_i}{\partial r} \right) = 0 \quad (6)$$

where  $c_i$  is the concentration of the species under consideration, i.e. the concentration of the metal ion, the reduced form of the redox couple or the oxidised form of the redox couple.  $D_i$  is the diffusion coefficient of species  $i$ ,  $r$  is the distance from the centre of the particle and  $t$  denotes the time from the beginning of growth. The initial conditions are:

$$c_i(r, t = 0) = c_i^{\text{b}} \quad (7)$$

where the superscript b denotes bulk concentration. The boundary conditions are given by:

$$\lim_{r \rightarrow \infty} c_i(r, t) = c_i^{\text{b}} \quad (8)$$

The fluxes at the surface of the particle can be related to its radius by noting that the flux of metal ions to the particle will be proportional to its rate of volume change. Thus, the growth rate is related to the concentration gradients at the surface as follows:

$$D_i \left. \frac{\partial c_i}{\partial r} \right|_{r=R(t)} = \frac{2n_{\text{M}}}{n_i \bar{V}} \frac{dR(t)}{dt} \quad (9)$$

where  $\bar{V}$  is the molar volume of the deposited phase and  $R(t)$  is the radius of the particle as a function of time. In the derivation of Eq. (9) it has been assumed that the diffusional fields can be partitioned symmetrically across the whole volume of the system, that is to

say regardless of the actual position of the particle at the interface. In this case half of the diffusional field will be present in the organic phase and the other half in the aqueous solution. The integration of Eq. (6) using conditions (7)–(9) leads to:

$$c_i(r, t) = c_i^{\text{b}} - \frac{n_{\text{M}}}{n_i} \frac{2R(t)^2}{r \bar{V} D_i} \frac{dR(t)}{dt} \quad (10)$$

Hence, from Eqs. (2) and (10) the relationship between the surface concentrations and the Galvani potential difference is given by:

$$\Delta_{\text{o}}^{\text{w}}\phi = E_{\text{Red/Ox}}^0 - E_{\text{M}^0/\text{M}^{n\text{M}}}^0 + \frac{RT}{n_{\text{M}} n_{\text{Red}} F} \times \ln \left[ \frac{\left( c_{\text{Ox}}^{\text{b}} + \frac{n_{\text{M}}}{n_{\text{Red}}} \frac{2R(t)}{\bar{V} D_{\text{Ox}}} \frac{dR(t)}{dt} \right)^{n_{\text{M}}}}{\left( c_{\text{Red}}^{\text{b}} - \frac{n_{\text{M}}}{n_{\text{Red}}} \frac{2R(t)}{\bar{V} D_{\text{Red}}} \frac{dR(t)}{dt} \right)^{n_{\text{M}}} \left( c_{\text{M}}^{\text{b}} - \frac{2R(t)}{\bar{V} D_{\text{M}}} \frac{dR(t)}{dt} \right)^{n_{\text{Red}}}} \right] \quad (11)$$

Eq. (11) is non-linear and a general solution in closed form for the radius as a function of interfacial potential and time could not be found. However, for a given set of bulk concentrations, the diffusional problem will have only one degree of freedom, i.e. when all initial conditions are given, there is only one function for the radius for a given potential and time.

### 2.1. Potentiostatic response for a single particle

If a function of the radius can be found such that the surface concentrations are constants with time, then this solution will also satisfy the condition of constant interfacial potential that is applied in a potentiostatic experiment. Setting  $r = R(t)$  in Eq. (10) gives the surface concentration of species  $i$  as:

$$c_i^{\sigma} = c_i^{\text{b}} - \frac{n_{\text{M}}}{n_i} \frac{2R(t)}{\bar{V} D_i} \frac{dR(t)}{dt} \quad (12)$$

where  $c_i^{\sigma}$  is the surface concentration, which is constant for a given potential. The radius of the particle is obtained by integration of Eq. (12) from zero to  $t$  under the condition that  $R(0) = 0$ :

$$R(t) = \left( \frac{n_i D_i \bar{V} (c_i^{\text{b}} - c_i^{\sigma}) t}{n_{\text{M}}} \right)^{1/2} = kt^{1/2} \quad (13)$$

From Eqs. (11) and (13):

$$\Delta_{\text{o}}^{\text{w}}\phi = E_{\text{Red/Ox}}^0 - E_{\text{M}^0/\text{M}^{n\text{M}}}^0 + \frac{RT}{n_{\text{M}} n_{\text{Red}} F} \times \ln \left[ \frac{\left( c_{\text{Ox}}^{\text{b}} + \frac{n_{\text{M}}}{n_{\text{Red}}} \frac{k^2}{\bar{V} D_{\text{Ox}}} \right)^{n_{\text{M}}}}{\left( c_{\text{Red}}^{\text{b}} - \frac{n_{\text{M}}}{n_{\text{Red}}} \frac{k^2}{\bar{V} D_{\text{Red}}} \right)^{n_{\text{M}}} \left( c_{\text{M}}^{\text{b}} - \frac{k^2}{\bar{V} D_{\text{M}}} \right)^{n_{\text{Red}}}} \right] \quad (14)$$

Although analytical expressions for the parameter  $k$  as a function of potential can be obtained from Eq. (14), a numerical solution through iteration is more convenient. For a sufficiently large overpotential the surface concentration of one reactant  $j$  (M or Red) can be considered to be zero. This is a limiting case for the growth rate and the parameter  $k$  written in terms of the limiting species  $j$  is obtained from Eq. (13) as:

$$k = \left( \frac{n_j c_j^b D_j \bar{V}}{n_M} \right)^{1/2} \quad (15)$$

In particular, when experimental conditions are chosen such that the surface concentration of the metal ion approaches zero ( $n_M D_M c_M^b \ll n_{\text{Red}} D_{\text{Red}} c_{\text{Red}}^b$ ) the parameter  $k$  is given by:

$$k = (c_M^b D_M \bar{V})^{1/2} \quad (16)$$

This result is similar to that obtained for a nucleus growing at a solid electrode [3]. However, in this case the parameter  $k$  differs by a factor of  $2^{1/2}$  due to the difference between the spherical and hemispherical geometry of the growing phase. The current to an isolated particle formed at  $t=0$  is obtained by solving the current density from Eqs. (9) and (13), using the relationship between the concentration gradient and the current, i.e.:

$$\left. \frac{\partial c_i}{\partial r} \right|_{r=R(t)} = \frac{I(t)}{n_i F A D_i} \quad (17)$$

from which the current is:

$$I(t) = \frac{2\pi n_M F k^3 t^{1/2}}{\bar{V}} \quad (18)$$

$I(t)$  is the current to a single particle.

## 2.2. Effect of overlapping diffusional fields

For nucleation and growth at a solid electrode, overlap of the diffusional fields around the nuclei takes place only in one phase. The situation at a liquid|liquid interface is more complicated, since overlap of the diffusional fields occurs in both phases, and therefore, a relationship between these overlapping fields must be established. The coupling between the diffusional fields leads to variable surface concentrations. Overlap will be treated using the concept of planar diffusion zones introduced by Gunawardena et al. [3] but the size of the planar diffusion zone will be defined in a different manner. Although there is a possibility of surface diffusion of particles at a liquid|liquid interface, their physical coalescence is neglected in the present model. The approach of planar diffusion zones requires that at least one surface concentration is constant. In the present derivation the current is calculated assuming a constant surface concentration for one reactant. The experimental condi-

tions for which the expressions obtained are valid are discussed later.

A planar linear diffusion zone of area  $S(t)$ , is defined so that the flux to this zone equals the radial flux to a single nucleus neglecting overlap [3]:

$$I_P(\tau) = I_R(\tau) \quad (19)$$

where  $I_P$  is the linear diffusion current to the planar diffusion zone,  $I_R$  is the current to the particle following hemispherical diffusion and  $\tau$  is the time elapsed since the formation of the nucleus. Following Scharifker's model [3], it will be considered that the area of the planar diffusion zone is assumed to grow linearly with time:

$$S(\tau) = \pi \alpha \tau \quad (20)$$

where  $\alpha$  is a parameter describing the growth rate of the diffusion zone. It will be shown in what follows that the assumption that  $\alpha$  is independent of time is correct. The current to an isolated particle formed at  $\tau=0$  is given by Eq. (18). The current due to linear flux to the growing planar diffusion zone is given by (see Appendix A for derivation):

$$I_P(\tau) = \frac{n_i F \Delta c_i D_i^{1/2}}{\pi^{1/2}} \int_0^\tau \frac{\partial S_i}{\partial u} \frac{du}{(\tau-u)^{1/2}} \quad (21)$$

where  $\Delta c_i = c_i^b - c_i^\sigma$  has been introduced for simplicity. Eq. (21) differs from the solution used in earlier studies [3–9]. The planar diffusion zone maps the real three-dimensional (3D) diffusion field of an independently growing nucleus into a hypothetical 2D diffusional field, where only diffusion perpendicular to the interfacial plane occurs. Previous studies [3–9] have related the current to the planar diffusion zone directly to the Cottrell equation, i.e. to a uniform diffusional layer over the whole diffusion zone initiated at  $\tau=0$ . However, as the mapped diffusion zone grows the time scale counted from the onset of the diffusion layer growth will shift, and hence the current to the hypothetical zone cannot be directly related by the Cottrell equation. In this study a solution is presented where a uniform diffusion layer inside the planar diffusion zone is not required. Eq. (21) is an exact solution of the current to the planar diffusion zone in the 2D case defined above, where no radial diffusion can occur, as the area grows.  $\alpha_i$  is solved from Eqs. (13), (18), (19) and (21) to yield:

$$\alpha_i = D_i \left( \frac{n_i}{n_M} \pi V \Delta c_i \right)^{1/2} \quad (22)$$

Thus the parameter  $\alpha$  is independent of time (Eq. (20)). To account for the overlap of the diffusional fields the total area fraction covered by the planar diffusion zones is calculated. Avrami [12] showed that the area fraction covered by randomly distributed circular areas can be related to the total area fraction covered by these neglecting overlap through:

$$\theta_i = 1 - \exp(-\theta_{\text{ex},i}) \quad (23)$$

where  $\theta_i$  and  $\theta_{\text{ex},i}$  denote the area fractions covered when accounting for and neglecting overlap of species  $i$ , respectively.  $\theta_{\text{ex},i}$  is given by the sum of the areas of the planar diffusion zones corresponding to all particles  $N(t)$  at time  $t$ :

$$\theta_{\text{ex},i} = \pi\alpha_i \int_0^t \frac{\partial N}{\partial u}(t-u)du \quad (24)$$

where  $N$  is the number density of nuclei as a function of time.  $\theta_{\text{ex},i}$  does not have the conventional meaning of an area fraction since its value is comprised between zero and infinity.

### 2.3. Nucleation rate law

A nucleation rate law is needed to calculate  $\theta_{\text{ex},i}$ . In contrast to the metal|solution interface, the liquid|liquid interface is assumed to be free from permanent nucleation sites. On a solid substrate the Gibbs energy of formation of nuclei is lower on these sites. An exponential nucleation rate law has commonly been used to describe the formation of new nuclei at solid electrodes [6]:

$$\frac{\partial N}{\partial t} = N_0 A \exp(-At) \quad (25)$$

where  $N_0$  is the maximum number of nuclei that can be formed on the surface and  $A$  is the nucleation rate constant. The extended area of species  $i$  is obtained from Eqs. (24) and (25) as [6]:

$$\theta_{\text{ex},i} = \pi\alpha_i N_0 \frac{At + \exp(-At) - 1}{A} \quad (26)$$

The physical meaning of  $N_0$  is different from that for a metal electrode since a finite number of nucleation sites is not necessarily present. This will be discussed later on. The rate of nucleation should be dependent on the supersaturation, i.e. the applied potential and the surface concentrations of the reactants at the liquid|liquid interface. In what follows, the nucleation model considered assumes that the rate of formation of new nuclei is constant at the surface fraction not covered by a planar diffusion zone and zero if it is covered. This corresponds to an exclusion-zone model in which the growing diffusional fields inhibits and eliminates nucleation in the exclusion region. The justification for this assumption is the strong dependence of nucleation rate on supersaturation. In this case, the growing diffusional hemispherical fronts will quench any further nucleation. Exclusion zones and local inhibition of nucleation rates have been treated both theoretically and have been shown in electrochemical nucleation experiments [13–15]. Serruya et al. [16] have shown that the exclusion zones are effectively equal to the

planar diffusion zones. From Eq. (23) the nucleation rate law is given by:

$$\frac{\partial N}{\partial t} = A(1 - \theta_i) = A \exp(-\theta_{\text{ex},i}) \quad (27)$$

where  $A$  is the nucleation rate constant and  $\theta_{\text{ex},i}$  is the extended coverage of species  $i$ . This rate law is dependent on the species considered. The conditions for which it is applicable are discussed later. From Eq. (24) with Eq. (27):

$$\theta_{\text{ex},i} = \pi\alpha_i A \int_0^t (t-u) \exp(-\theta_{\text{ex},i}) du \quad (28)$$

Since  $(t-u) \exp(-\theta_{\text{ex},i})$  and its derivative with respect to  $t$  are continuous functions Eq. (28) can be reduced to a differential equation [17], i.e.:

$$\frac{\partial^2 \theta_{\text{ex},i}}{\partial t^2} = \pi\alpha_i A \exp(-\theta_{\text{ex},i}) \quad (29)$$

with the following initial and boundary conditions:

$$\theta_{\text{ex},i}(0) = 0 \quad (30)$$

and

$$\left. \frac{\partial \theta_{\text{ex},i}}{\partial t} \right|_{t=0} = 0 \quad (31)$$

Differential (29) is solved by separation of variables (Appendix B), and the area fraction neglecting overlap is given by:

$$\theta_{\text{ex},i}(t) = 2 \ln \left( \frac{\exp(-(2\pi\alpha_i A)^{1/2} t) + 1}{2} \right) + (2\pi\alpha_i A)^{1/2} t \quad (32)$$

### 2.4. Final equations

The current density to the interface is obtained by calculating the linear flux to the area fraction covered by the planar diffusion zones accounting for their growth. Thus, similar to Eq. (21) (Appendix A), the current density is given by:

$$j(t) = \frac{n_i F \Delta c_i D_i^{1/2}}{\pi^{1/2}} \int_0^t \frac{\partial \theta_i}{\partial u} \frac{du}{(t-u)^{1/2}} \quad (33)$$

Eq. (33) can be integrated for the two nucleation rate cases previously discussed. For the exponential rate law:

$$\frac{\partial \theta_i}{\partial u} = \pi\alpha_i N_0 (\exp(-At) - 1) \exp \left( \frac{\pi\alpha_i N_0 (At - 1 + \exp(-At))}{A} \right) \quad (34)$$

and for the exclusion-progressive rate law (Appendix B):

$$\frac{\partial \theta_i}{\partial u} = \frac{4(2\pi\alpha_i A)^{1/2} \exp(-2\pi\alpha_i A)^{1/2} u (1 - \exp(-2\pi\alpha_i A)^{1/2} u)}{(1 + \exp(-2\pi\alpha_i A)^{1/2} u)^3} \quad (35)$$

The parameter  $\alpha_i$  is given by Eq. (22). The current density (Eq. (33)) has to be numerically evaluated for both rate laws (Eqs. (34) and (35)). These equations are also valid for nucleation at solid electrodes if  $\alpha$  (Eq. (22)) is multiplied by  $2^{3/2}$  to account for the difference in the symmetry of the growing phase.

### 2.5. The constant surface concentration prerequisite

This section is intended to show that overlap can lead to variable surface concentrations at a particle growing under potentiostatic conditions and to deduce the conditions in which the derived model applies. Flux continuity requires that the current given by Eq. (33) for two different species are equal, e.g. for M and Red:

$$\frac{n_{\text{Red}} F \Delta c_{\text{Red}} D_{\text{Red}}^{1/2}}{\pi^{1/2}} \int_0^t \frac{\partial \theta_{\text{Red}}}{(t-u)^{1/2}} du = \frac{n_{\text{M}} F \Delta c_{\text{M}} D_{\text{M}}^{1/2}}{\pi^{1/2}} \int_0^t \frac{\partial \theta_{\text{M}}}{(t-u)^{1/2}} du \quad (36)$$

where  $\theta_{\text{Red}}$  and  $\theta_{\text{M}}$  denote the coverage of the interface by the respective species. From the Avrami theorem (23), the expressions for  $\theta_{\text{ex}}$  (Eq. (24)) and Eq. (36) yield:

$$\frac{n_{\text{Red}} F \Delta c_{\text{Red}} D_{\text{Red}}^{1/2} \pi^{1/2} \alpha_{\text{Red}}}{\pi^{1/2}} \int_0^t \frac{N(u) \exp\left(-\pi \alpha_{\text{Red}} \int_0^u \frac{\partial N}{\partial w} (u-w) dw\right)}{(t-u)^{1/2}} du = \frac{n_{\text{M}} F \Delta c_{\text{M}} D_{\text{M}}^{1/2} \pi^{1/2} \alpha_{\text{M}}}{\pi^{1/2}} \int_0^t \frac{N(u) \exp\left(-\pi \alpha_{\text{M}} \int_0^u \frac{\partial N}{\partial w} (u-w) dw\right)}{(t-u)^{1/2}} du \quad (37)$$

It follows from the expression for  $\alpha_i$  (Eq. (22)) that the value of the constant in front of the integral is independent of the species considered. The definition of  $\alpha_i$  includes the assumption that the surface concentrations are constant. The only difference between the left and right hand sides of Eq. (37) is in the exponential

terms in the parameters  $\alpha_i$ , and hence these must have the same value independently of the species considered. Thus, equating Eq. (22) for M and Red and simplifying gives:

$$n_{\text{Red}} D_{\text{Red}}^{1/2} \Delta c_{\text{Red}} = n_{\text{M}} D_{\text{M}}^{1/2} \Delta c_{\text{M}} \quad (38)$$

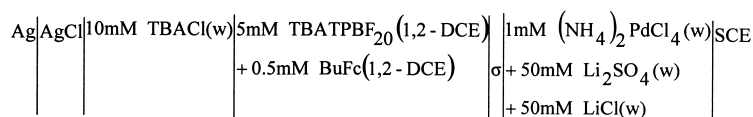
The surface concentrations of the planar diffusion zone are, by definition, equal to the surface concentrations of the particle. Thus, the surface concentrations can be solved from Eq. (12). Substituting the expressions for  $\Delta c_i$  into Eq. (38) and simplifying gives:

$$D_{\text{Red}} = D_{\text{M}} \quad (39)$$

This implies that the surface concentrations are constants only if the diffusion coefficients are equal. Qualitatively, this is explained by the different degrees of overlap resulting from different diffusion coefficients. Different degrees of overlap result in different mass transport efficiencies, and hence the surface concentrations must vary to maintain flux continuity. However, a quasi-constant surface concentration can be achieved if a large potential step is applied so that the surface concentration of one species approaches zero and the surface concentrations of the other species are large. This condition occurs, for example, when  $n_{\text{Red}} D_{\text{Red}} c_{\text{Red}}^b \ll n_{\text{M}} D_{\text{M}} c_{\text{M}}^b$ . In this case, changes in the absolute values of the surface concentrations required for flux continuity will occur in the species with high surface concentrations, and hence the absolute value of the surface concentration of the limiting species can be considered as constant. The supersaturation will also be determined by this limiting species, and hence the rate law derived for the liquid | liquid interface is also applicable. Stewart et al. [18] have discussed similar situations in connection to cyclic voltammetry and electron transfer at liquid | liquid interfaces. It follows from this condition that  $\Delta c_i = c_i^b$  in Eq. (33).

### 3. Experimental

A typical four-electrode cell configuration for the liquid | liquid interface was used [19]. The potential was controlled and recorded using an Autolab PGStat 100 (Ecochemie, Netherlands) potentiostat controlled by a PC. The cell configuration shown in Cell 1 was used:



(Cell 1)

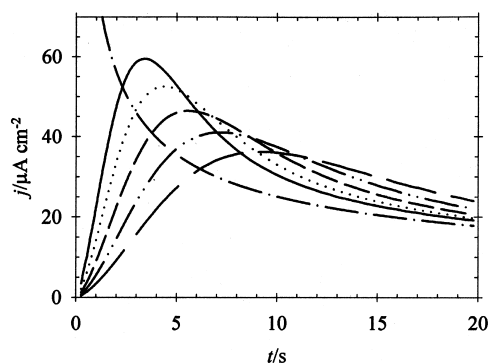


Fig. 3. Calculated transients for the exclusion-progressive rate law. The organic redox species was chosen as the limiting species. The following values were used:  $n_M = 2$ ,  $n_{\text{Red}} = 1$ ,  $D_{\text{Red}} = 0.83 \times 10^{-5} \text{ cm}^2 \text{ s}^{-1}$ ,  $\bar{V} = 9.33 \text{ cm}^3 \text{ mol}^{-1}$  and  $c_{\text{Red}}^b = 0.5 \times 10^{-6} \text{ mM}$ . The transients were plotted for the following nucleation rates:  $A = 3.28 \times 10^6$  (—),  $2.00 \times 10^6$  (···),  $1.22 \times 10^6$  (---),  $0.75 \times 10^6$  (-·-·-) and  $0.46 \times 10^6 \text{ cm}^{-2} \text{ s}^{-1}$  (— — —). The Cottrell transient (-·-·-) is also presented for the same parameters.

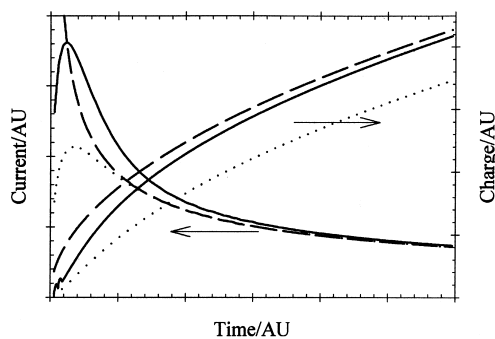


Fig. 4. Calculated transients and the corresponding deposition charges for instantaneous nucleation. The results refer to: (—) the model derived in this study, Eq. (40), (···) the model by Gunawardena et al. [3], (-·-·-) the Cottrell transient.

where  $\sigma$  denotes the interface studied. A positive current is defined as transfer of a positive charge from the aqueous phase to the organic phase. 1,2-Dichloroethane (1,2-DCE) (HPLC grade Rathburn Chemicals, Scotland),  $\text{Li}_2\text{SO}_4$ ,  $\text{LiCl}$  and  $(\text{NH}_4)_2\text{PdCl}_4$  (Aldrich, USA) were used without further purification. Butylferrocene (BuFc) (Aldrich, USA) was the electron donor in the organic phase. MQ-treated water was used throughout. Tetrabutylammoniumtetrakis(pentafluorophenyl)borate ( $\text{TBATPBF}_{20}$ ) was prepared by metathesis of tetrabutylammoniumchloride (TBACl) and lithiumtetrakis(pentafluorophenyl)borate ( $\text{LiTPBF}_{20}$ ) in 2:1 mixtures of methanol and water, followed by recrystallisation in acetone [20]. The applied potentials were transformed to the Galvani scale as described elsewhere using  $\Delta_\sigma^w \phi_{\text{TBA}^+}^0 = -225 \text{ mV}$  [21]. The system was studied by cyclic voltammetry and potential step techniques. For the potential step experiments the potential was initially set at  $\Delta_\sigma^w \phi = 49 \text{ mV}$  and stepped to the range from 249 to 299 mV with a 12.5 mV interval. The cell

was cleaned after each potential step measurement to ensure a clean interface.

## 4. Results and discussion

### 4.1. Model predictions

The transients predicted for the exclusion-progressive rate law calculated from Eqs. (33) and (35), for a large potential step where  $\Delta c_i = c_{\text{Red}}^b$ , are plotted for several nucleation rate constants in Fig. 3. The plots are for a diffusion coefficient of  $0.83 \times 10^{-5} \text{ cm}^2 \text{ s}^{-1}$  for butylferrocene and a molar volume of  $9.33 \text{ cm}^3 \text{ mol}^{-1}$  [22] for palladium. At short times the approximation  $\theta = 1 - \exp(-\theta_{\text{ex}}) \approx \theta_{\text{ex}}$  can be used and consequently, from the definition of  $\theta_{\text{ex}}$  it follows that the current at short times corresponds to individually growing nuclei. At long times the expected Cottrell behaviour, corresponding to linear diffusion resulting from the overlap of the spherical diffusional fields is observed.

Fig. 4 compares the transients and deposition charges for the instantaneous nucleation case for the Scharifker model and for the model developed here. These transients were calculated for a solid electrode from Eq. (12) in Gunawardena et al. [3] and Eqs. (23), (24) and (33) by setting  $N(t) = H(t)N_0$  where  $H(t)$  is the unit step function. The latter simplifies Eq. (33) to:

$$j(t) = 2nFc_i^b(\alpha_i D_i N_0)^{1/2} \Phi((\pi \alpha_i N_0 t)^{1/2}) \quad (40)$$

where  $\Phi$  denotes Dawson's integral. The parameter  $\alpha$  (Eq. (22)) was corrected for the different growth symmetries by multiplying with  $2^{3/2}$ . The transient for the model derived in this study crosses the Cottrell transient. The deposition charges are also shown in this Fig. 4. The transient corresponding to the Scharifker model does not cross the Cottrell transient and therefore the deposition charge is systematically smaller than that derived from the Cottrell equation. This error stems from the quasi-stationary assumption that the electrode coverage and the area of the planar diffusion zones are constant when the current is solved (see text referring to Eq. (21) and Appendix A). The result of this assumption is that the current is underestimated since the current density to any point in the area covered is related to  $t = 0$  instead of the actual time at which it was covered. As expected, the deposition charge of the present model reaches that of the Cottrell transient at long times.

There has been some controversy regarding the applicability of the concept of planar diffusion zones for the description of current transients for nucleation with 3D diffusion controlled growth [6]. The approximation of planar diffusion fields should be verified not only by measurements but also using computer simulations. Unfortunately, no such rigorous studies, with random

distribution of nuclei and non-instantaneous nucleation, have been presented. Nagy and Denuault [23] performed a series of random walk simulations for an instantaneous nucleation process at an ordered square lattice. Although the latter is experimentally very unlikely, it gives at least the qualitative features also applicable to a random distribution of nuclei. For instance, the current transient was found to cross that of the corresponding Cottrell transient and at long times asymptotically approach the Cottrell transient. The model presented here also predicts these features.

#### 4.2. Experimental results

Finding a suitable experimental system for electrochemical studies of nucleation processes at liquid|liquid interfaces is difficult due to the sensitivity of nucleation phenomena to the presence of adventitious nucleation sites, e.g. resulting from spontaneous deposition of particles at the interface. This can result from coupling between ion and electron transfer. The system

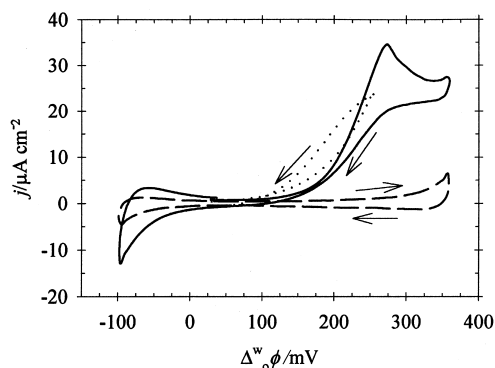


Fig. 5. Cyclic voltammograms for Cell 1 obtained at a sweep rate of  $25 \text{ mV s}^{-1}$ . (---)  $0.5 \text{ mM BuFc (1,2-DCE)} + 5 \text{ mM TBATPBF}_{20} \text{ (1,2-DCE)}$  in contact with  $100 \text{ mM LiCl} + 100 \text{ mM Li}_2\text{SO}_4 \text{ (H}_2\text{O)}$ . (—) as before but with the addition of  $1.0 \text{ mM (NH}_4\text{)}_2\text{PdCl}_4$  to the aqueous phase. (···) represents a voltammetric scan reversed at a potential less positive than the peak potential featuring a clear nucleation loop.

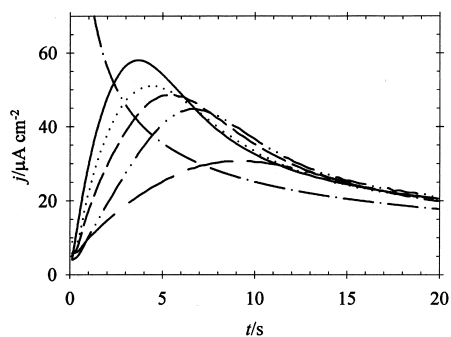


Fig. 6. Experimental transients at the following potentials for the system described in Cell 1:  $299 \text{ mV}$  (—),  $286.5 \text{ mV}$  (···),  $274 \text{ mV}$  (---),  $261.5 \text{ mV}$  (-·-·-) and  $249 \text{ mV}$  (— — —). The Cottrell transient (— · — ·) was calculated as in Fig. 3.

used in this study also leads to a spontaneous deposition. However, this was very slow and the reproducibility of the transients observed indicates that the effect on the results is small. The spontaneous reaction rate was found to decrease with increasing pH. Slow precipitation of palladium oxide was observed at  $\text{pH} > 7$ . The pH of the solution was buffered at 5.3. The sulfate/bisulfate buffer does not form complexes with palladium. LiCl was added to the base electrolyte to stabilise the palladate complex. The spontaneous reduction of the palladium ion could, however, not be completely stopped and a black precipitate could be observed after two days of contacting the two phases at open circuit. This spontaneous reaction is slow enough not to affect the observed current transients, provided that the potential step is performed rapidly after the solutions are brought into contact. However, if the system was allowed to stand for longer than 20 min with the solutions in contact prior to the application of the potential step, the shape of the transient was significantly affected, shifting the peak position to shorter times and introducing Cottrell character at the beginning of the transient due to the presence of particles at the interface before the potential step.

Fig. 5 shows cyclic voltammograms for the electrochemical reduction of  $\text{PdCl}_4^{2-}$  at the water|1,2-DCE interface. When only the aqueous or organic redox couple was present, the voltammogram followed the base line, indicating that the redox couples themselves are not transferring in the polarisation window. When both the organic redox species and the aqueous ammonium palladate solutions were present an irreversible reduction peak was observed, with a Galvani peak potential of  $\Delta\phi_p^w = 273 \text{ mV}$ . In this case the currents at the negative end of the scan were slightly larger than those observed in the absence of Pd(II), due to the transfer of the butylferrocenium ion formed in the deposition reaction. Fig. 5 also shows that when the scan was reversed at a less positive potential, before the onset of linear diffusion, a typical nucleation loop was observed with higher currents on the reverse sweep than on the forward sweep.

Fig. 6 shows the current transient responses to a potential step experiment. All the measurements were performed by first applying a potential of  $49 \text{ mV}$  for  $30 \text{ s}$ , where no electrochemical deposition occurs and then stepping to the desired potential. These transients are characteristic of a typical nucleation and growth process. The increase of the current corresponds to a growing reaction area, whereas the following decrease is due to the onset of linear diffusion conditions. As predicted by the theory, the transients reach a maximum that is larger than the theoretical Cottrell response calculated with a diffusion coefficient of  $0.83 \times 10^{-5} \text{ cm}^2 \text{ s}^{-1}$  for butylferrocene. This diffusion coefficient was obtained from microelectrode measurements. In addition, the theory predicts that the tran-

Table 1  
Nucleation rate  $A$  and  $N_\infty$  obtained from the exclusion-progressive rate law

| $\Delta\phi^w/mV$ | $10^{-6} A/cm^2 s^{-1}$ | $10^{-6} N_\infty/cm^2 s^{-1}$ |
|-------------------|-------------------------|--------------------------------|
| 299               | 3.28                    | 9.63                           |
| 261.5             | 2.00                    | 7.52                           |
| 274               | 1.22                    | 5.88                           |
| 261.6             | 0.75                    | 4.59                           |
| 249               | 0.46                    | 3.59                           |

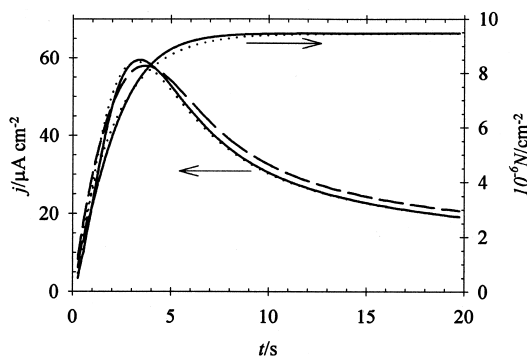


Fig. 7. Comparison of theoretical transients and nuclear number densities obtained for the different rate laws; (—) exclusion-progressive, (···) exponential rate law and (---) the experimental transient obtained at 299 mV.

sient of a step performed to a less positive potential crosses that of a step performed to a more positive potential after the peak. This is also observed in the experimental results. However, the currents recorded at the least positive potentials were slightly smaller than expected. This is likely to be due to increased surface concentration of the limiting reactant at less positive potentials.

The transient obtained with the largest potential step was fitted to the exclusion-progressive nucleation rate law by a method of trial and error. The rest of the transients were well fitted by applying an exponential relation between the applied potential and the nucleation rate. The activation energy predicted from classical nucleation theory [24], which equates the Gibbs energy of the critical nucleus to the activation energy for nucleation predicts a linear relation between the logarithm of the nucleation rate and the inverse square of the applied potential. However, atomistic theory predicts a linear relationship between the logarithm of the nucleation rate and the applied potential [25]. The obtained rate constants and number of nuclei (Eq. (B15)) are given in Table 1.

The experimental transients can also be successfully fitted to the theory if the exponential rate law is used instead of the exclusion-progressive rate law. As shown in Fig. 7 the number of nuclei as a function of time is

very similar to that obtained from the exclusion-progressive rate law. Although  $N_0$  is related to a physical nucleation preferential site, similar parameters as  $N_0$  in Eqs. (25) and (26) can still be defined on the basis of the exclusion zone model discussed here (Eq. (B15)). The overall nucleation rate decreases markedly in the same time range at which the current peak occurs. This indicates that the physical reason for the decay of the overall nucleation rate is a decrease of the average interfacial surface concentrations and hence, the supersaturation. This is an indication that the liquid | liquid interface is free from preferential nucleation sites, and in this sense ideal for nucleation studies.

## 5. Conclusions

A model for diffusion controlled nucleation at the liquid | liquid interface, based on the model developed by Scharifker and co-workers [3–5] has been presented. This model cannot be applied to all experimental conditions since the coupled diffusional fields in the two phases lead to variable surface concentrations. Thus, there is a need for a more general approach to model diffusion controlled nucleation processes. The nucleation process at the liquid | liquid interface has been shown to be different from that at solid electrodes, as the results indicate that the interface is free from preferential nucleation sites. In addition, the nucleation rate was found to depend exponentially on the applied voltage.

## Acknowledgements

The author gratefully acknowledge the National Technology Agency (Finland) and the EU TMR network Project: Organization Dynamics and Reactivity at Electrified Liquid | Liquid Interfaces (TMR Contract ERBFMRXCT960078).

## Appendix A. Derivation of current by linear diffusion to a growing area

The differential equation system for linear flux to a growing area can be written as:

$$D \frac{\partial^2 c((x^\sigma, y^\sigma), z, t)}{\partial z^2} = \frac{\partial c((x^\sigma, y^\sigma), z, t)}{\partial t} \quad (A1)$$

$$c((x^\sigma, y^\sigma), z, t = 0) = c^b \quad (A2)$$

$$\lim_{z \rightarrow \infty} c((x^\sigma, y^\sigma), z, t) = c^b \quad (A3)$$

$$c((x^\sigma, y^\sigma), z = 0, t) = c^b - \Delta c H(t - t_0(x^\sigma, y^\sigma)) \quad (A4)$$

where  $(x^\sigma, y^\sigma)$  is a coordinate in the interfacial plane,  $z$  is the distance from this plane and  $H$  is the Heaviside unit step function. This differential equation system

arises from the definition of the planar diffusion zones, where the 3D diffusion problem is reduced to two dimensions. When a coordinate is covered by a planar diffusion zone its surface concentration changes by  $\Delta c$ , from  $c^b$  to  $c^\sigma$ . The function  $t_0(x^\sigma, y^\sigma)$  describes the time of onset of linear diffusion as a function of coordinate  $(x^\sigma, y^\sigma)$  on the interfacial plane. Hence,  $t - t_0(x^\sigma, y^\sigma)$  is the time elapsed from the onset of the linear flux to this coordinate. The surface concentration is schematically presented in Fig. 8 for an arbitrary area.

Application of conditions (A2) and (A3) to the Laplace transformation of Eq. (A1) gives:

$$\bar{C}((x^\sigma, y^\sigma), z, s) = \frac{c^b}{s} + \bar{F}((x^\sigma, y^\sigma), s) \exp\left(-\left(\frac{s}{D}\right)^{1/2} z\right) \quad (\text{A5})$$

where  $\bar{F}((x^\sigma, y^\sigma), s)$  is an integration constant with respect to  $z$  and is solved from boundary condition (A4):

$$\bar{C}((x^\sigma, y^\sigma), 0, s) = \frac{c^b}{s} - \Delta c \frac{\exp(-st_0(x^\sigma, y^\sigma))}{s} \quad (\text{A6})$$

The concentration profile is obtained from Eqs. (A5) and (A6) as:

$$\bar{C}((x^\sigma, y^\sigma), z, s) = \frac{c^b}{s} - \frac{\Delta c}{s} \exp(-st_0(x^\sigma, y^\sigma)) \exp\left(-\left(\frac{s}{D}\right)^{1/2} z\right) \quad (\text{A7})$$

The current density is obtained from the gradient at  $z = 0$ :

$$j((x^\sigma, y^\sigma), t) = nFD^{1/2}\Delta c \frac{\exp(-st_0(x^\sigma, y^\sigma))}{s^{1/2}} \quad (\text{A8})$$

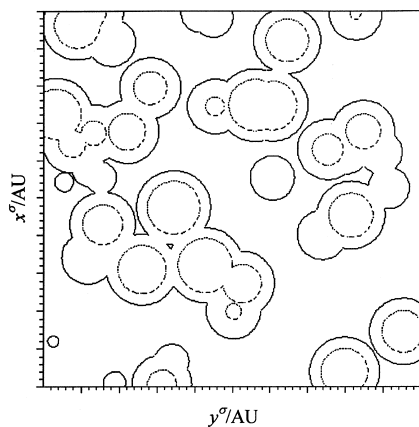


Fig. 8. Schematic representation of growing planar diffusion zones at two different times; (---) at  $t_0$  and (—) at  $t_2$ , where  $t_2 > t_1$ . The concentration is defined as  $c^\sigma$  inside and  $c^b$  outside the planar diffusion zones. With time the diffusion zones overlap and the covered area acquires arbitrary shape. This behaviour of the interfacial concentration is described by Eq. (A4). The schematic diffusion zones are distributed in time and space according to the exclusion-progressive rate law.

Inverse transformation of Eq. (A8) gives the current density to the coordinate  $(x^\sigma, y^\sigma)$  as a function of time:

$$j((x^\sigma, y^\sigma), t) = \frac{nFD^{1/2}\Delta c}{\pi^{1/2}} \frac{H(t - t_0(x^\sigma, y^\sigma))}{(t - t_0(x^\sigma, y^\sigma))^{1/2}} \quad (\text{A9})$$

The total current to the growing area is given by integration of the current density over the surface  $S$ :

$$I_p(t) = \int j((x^\sigma, y^\sigma), t) dS \quad (\text{A10})$$

Combining Eq. (A9) with (A10) and defining  $u = t_0(x^\sigma, y^\sigma)$  gives:

$$I_p(t) = \frac{nFD^{1/2}\Delta c}{\pi^{1/2}} \int_0^t \frac{\frac{\partial S}{\partial u} du}{(t-u)^{1/2}} \quad (\text{A11})$$

where the fact that the current density is zero when  $t < t_0(x^\sigma, y^\sigma)$  has been used to obtain the upper integration limit.

## Appendix B. Derivation of exclusion-progressive rate law

The exclusion-progressive rate law is derived from Eq. (29):

$$\frac{\partial^2 \theta_{\text{ex}}}{\partial t^2} = \pi\alpha A \exp(-\theta_{\text{ex}}) \quad (\text{B1})$$

Let us define:

$$p = \frac{\partial \theta_{\text{ex}}}{\partial t} \quad (\text{B2})$$

Application of the chain rule gives the derivative of  $p$ :

$$\frac{\partial p}{\partial t} = \frac{\partial p}{\partial \theta_{\text{ex}}} \frac{\partial \theta_{\text{ex}}}{\partial t} = p \frac{\partial p}{\partial \theta_{\text{ex}}} \quad (\text{B3})$$

Substitution of Eq. (B3) into Eq. (B1) gives:

$$p \frac{\partial p}{\partial \theta_{\text{ex}}} = \pi\alpha A \exp(-\theta_{\text{ex}}) \quad (\text{B4})$$

Solving for  $p$  by separation of variables and integration gives:

$$1/2p^2 + C_1 = -\pi\alpha A \exp(-\theta_{\text{ex}}) \quad (\text{B5})$$

from which  $p$  is solved:

$$p = \frac{\partial \theta_{\text{ex}}}{\partial t} = (-2\pi\alpha A \exp(-\theta_{\text{ex}}) - 2C_1)^{1/2} \quad (\text{B6})$$

Separation of variables of Eq. (B6) gives:

$$t + C_2 = \int \frac{d\theta_{\text{ex}}}{(-2\pi\alpha A \exp(-\theta_{\text{ex}}) - 2C_1)^{1/2}} \quad (\text{B7})$$

This integral can be written on the following form by defining  $x = \exp(-\theta_{\text{ex}})$ :

$$F = \int \frac{dx}{(a + bx)^{1/2}x} \quad (\text{B8})$$

to which the solution is given by Weast [22]. Hence, the solution to Eq. (B8) is:

$$\theta_{\text{ex}}(t) = \ln \left( - \frac{\pi\alpha A}{C_1 \tan \left( \frac{(2C_1)^{1/2}t + (2C_1)^{1/2}C_2}{2} \right) + C_1} \right) \quad (\text{B9})$$

Initial conditions (30) and (31) give the integration constants as  $C_1 = -\pi\alpha A$  and  $C_2 = \theta$ :

$$\theta_{\text{ex}}(t) = \ln \left( \frac{\pi\alpha A}{\pi\alpha A \tan \left( \frac{(-2\pi\alpha A)^{1/2}t}{2} \right) + \pi\alpha A} \right) \quad (\text{B10})$$

Converting the tangent in Eq. (B10) to exponential form and simplifying yields:

$$\theta_{\text{ex}}(t) = 2 \ln \left( \frac{\exp(- (2\pi\alpha A)^{1/2}t) + 1}{2} \right) + (2\pi\alpha A)^{1/2}t \quad (\text{B11})$$

From Eqs. (B11) and (27) the actual coverage is obtained as:

$$\begin{aligned} \theta(t) &= 1 - \exp \left( -2 \ln \left( \frac{\exp(- (2\pi\alpha A)^{1/2}t) + 1}{2} \right) \right. \\ &\quad \left. - (2\pi\alpha A)^{1/2}t \right) \end{aligned} \quad (\text{B12})$$

Derivation of Eq. (B12) with respect to  $t$ :

$$\begin{aligned} \frac{\partial \theta}{\partial t} &= 4 \frac{(2\pi\alpha A)^{1/2} \exp(- (2\pi\alpha A)^{1/2}t) (1 - \exp(- (2\pi\alpha A)^{1/2}t))}{(1 + \exp(- (2\pi\alpha A)^{1/2}t))^3} \end{aligned} \quad (\text{B13})$$

The number of nuclei as a function of time is obtained from Eqs. (31) and (B12) as:

$$N(t) = 2 \frac{(2A)^{1/2}}{(\pi\alpha)^{1/2} (\exp(- (2\pi\alpha A)^{1/2}t) + 1)} - \left( \frac{2A}{\pi\alpha} \right)^{1/2} \quad (\text{B14})$$

This rate law gives a finite number of nuclei as  $t \rightarrow \infty$ :

$$N_{\infty} = \left( \frac{2A}{\pi\alpha} \right)^{1/2} \quad (\text{B15})$$

## References

- [1] Y. Cheng, D.J. Schiffrin, *J. Chem. Soc. Faraday Trans.* 92 (1996) 3865.
- [2] R. Greef, R. Peat, L.M. Peter, D. Pletcher, J. Robinson, *Instrumental Methods in Electrochemistry*, Ellis Horwood, Chichester, 1985, p. 283.
- [3] G. Gunawardena, G. Hills, I. Montenegro, B. Scharifker, *J. Electroanal. Chem.* 138 (1982) 225.
- [4] B. Scharifker, G. Hills, *Electrochim. Acta* 28 (1983) 879.
- [5] B. Scharifker, J. Mostany, *J. Electroanal. Chem.* 177 (1984) 13.
- [6] L. Heerman, A. Tarallo, *J. Electroanal. Chem.* 470 (1999) 70.
- [7] M.V. Mirkin, A.P. Nilov, *J. Electroanal. Chem.* 283 (1990) 31.
- [8] M. Sluyters-Rehbach, J.H.O.J. Wijenbergh, E. Bosco, J.H. Sluyters, *J. Electroanal. Chem.* 236 (1987) 1.
- [9] B.R. Scharifker, J. Mostany, M. Palomar-Pardavé, I. Gonzalez, *J. Electrochem. Soc.* 146 (1999) 1005.
- [10] V.J. Cunnane, D.J. Schiffrin, C. Beltran, G. Geblewicz, T. Solomon, *J. Electroanal. Chem.* 247 (1988) 203.
- [11] R. Ahlrichs, S.D. Elliot, *Phys. Chem. Chem. Phys.* 1 (1999) 13.
- [12] M. Avrami, *J. Chem. Phys.* 7 (1939) 1103.
- [13] E. Garcia-Pastoriza, J. Mostany, B.R. Scharifker, *J. Electroanal. Chem.* 441 (1998) 13.
- [14] B.R. Scharifker, J. Mostany, A. Serruya, *Electrochim. Acta* 37 (1992) 2503.
- [15] A. Milchev, W.S. Krujic, M. Sluyters-Rehbach, J.H. Sluyters, *J. Electroanal. Chem.* 362 (1993) 21.
- [16] A. Serruya, J. Mostany, B.R. Scharifker, *J. Chem. Soc. Faraday Trans.* 89 (1993) 255.
- [17] F.B. Hildebrand, *Methods of Applied Mathematics*, second ed., Prentice-Hall, Englewood Cliffs, NJ, 1952, p. 223.
- [18] A.A. Stewart, J.A. Campbell, H.H. Girault, *Ber. Bunsenges. Phys. Chem.* 94 (1990) 83.
- [19] Z. Samec, V. Marecek, J. Koryta, M.W. Khalil, *J. Electroanal. Chem.* 83 (1977) 393.
- [20] D.J. Fermín, H.D. Duong, Z. Ding, P.-F. Brevet, H.H. Girault, *Phys. Chem. Chem. Phys.* 1 (1999) 1461.
- [21] J. Czapkiewicz, B. Czapkiewicz-Tutaj, *J. Chem. Soc. Faraday Trans.* 76 (1980) 1663.
- [22] R.W. Weast, *CRC Handbook of Chemistry and Physics*, CRC Press, Boca Raton, FL, 1980, A-52, B-126.
- [23] G. Nagy, G. Denuault, *J. Electroanal. Chem.* 433 (1997) 175.
- [24] A. Milchev, S. Stoyanov, *J. Electroanal. Chem.* 72 (1976) 33.
- [25] A. Milchev, E. Vassileva, *J. Electroanal. Chem.* 107 (1980) 337.